

# New determination of the mass of the $\eta$ meson at COSY-ANKE

P. Goslawski,<sup>1,\*</sup> A. Khoukaz,<sup>1,†</sup> S. Barsov,<sup>2</sup> I. Burmeister,<sup>1</sup> D. Chiladze,<sup>3,4</sup> S. Dymov,<sup>5,6</sup>  
R. Gebel,<sup>3</sup> M. Hartmann,<sup>3</sup> A. Kacharava,<sup>3</sup> P. Kulesa,<sup>7</sup> A. Lehrach,<sup>3</sup> B. Lorentz,<sup>3</sup> R. Maier,<sup>3</sup>  
T. Mersmann,<sup>1</sup> M. Mielke,<sup>1</sup> S. Mikirtychiants,<sup>3,2</sup> H. Ohm,<sup>3</sup> M. Papenbrock,<sup>1</sup> D. Prasuhn,<sup>3</sup>  
T. Rausmann,<sup>1</sup> V. Serdyuk,<sup>6</sup> H. Stockhorst,<sup>3</sup> H. Ströher,<sup>3</sup> A. Täschner,<sup>1</sup> Yu. Valdau,<sup>3,8</sup> and C. Wilkin<sup>9</sup>

<sup>1</sup>*Institut für Kernphysik, Universität Münster, D-48149 Münster, Germany*

<sup>2</sup>*High Energy Physics Department, Petersburg Nuclear Physics Institute, RU-188350 Gatchina, Russia*

<sup>3</sup>*Institut für Kernphysik and Jülich Centre for Hadron Physics,  
Forschungszentrum Jülich, D-52425 Jülich, Germany*

<sup>4</sup>*High Energy Physics Institute, Tbilisi State University, GE-0186 Tbilisi, Georgia*

<sup>5</sup>*Physikalisches Institut, Universität Erlangen-Nürnberg, D-91058 Erlangen, Germany*

<sup>6</sup>*Laboratory of Nuclear Problems, JINR, RU-141980 Dubna, Russia*

<sup>7</sup>*H. Niewodniczanski Institute of Nuclear Physics PAN, PL-31342 Cracow, Poland*

<sup>8</sup>*Helmholtz-Institut für Strahlen- und Kernphysik, Universität Bonn, D-53115 Bonn, Germany*

<sup>9</sup>*Physics and Astronomy Department, UCL, Gower Street, London WC1E 6BT, U.K.*

(Dated: May 31, 2018)

A value for the mass of the  $\eta$  meson has been determined at the COSY-ANKE facility through the measurement of a set of deuteron laboratory beam momenta and associated  ${}^3\text{He}$  center-of-mass momenta in the  $dp \rightarrow {}^3\text{He}X$  reaction. The  $\eta$  was then identified by the missing-mass peak and the production threshold determined. The individual beam momenta were fixed with a relative precision of  $3 \times 10^{-5}$  for values around 3 GeV/c by using a polarized deuteron beam and inducing an artificial depolarizing spin resonance, which occurs at a well-defined frequency. The final-state momenta in the two-body  $dp \rightarrow {}^3\text{He}\eta$  reaction were investigated in detail by studying the size of the  ${}^3\text{He}$  momentum ellipse with the forward detection system of the ANKE spectrometer. Final alignment of the spectrometer for this high precision experiment was achieved through a comprehensive study of the  ${}^3\text{He}$  final-state momenta as a function of the center-of-mass angles, taking advantage of the full geometrical acceptance. The value obtained for the mass,  $m_\eta = (547.873 \pm 0.005_{\text{stat}} \pm 0.027_{\text{syst}})$  MeV/c<sup>2</sup>, is consistent and competitive with other recent measurements, in which the meson was detected through its decay products.

PACS numbers: 13.75.-n, 14.40.Be

## I. INTRODUCTION

The precise value of the mass of the  $\eta$  meson has been the subject of intense debate for several years. The situation seems to have been finally resolved with the publication of four experiments that obtained consistent results to high accuracy [1–4]. In all these new experiments the meson was cleanly identified through one or more of its decay modes,  $\pi^0\pi^0\pi^0$  [1],  $\gamma\gamma$  [2], or both [3], or these plus  $\pi^+\pi^-\pi^0$  and  $\pi^+\pi^-\gamma$  [4]. Taking only decay experiments into account, the Particle Data Group now quote their “best” estimate of the mass as being  $m_\eta = (547.853 \pm 0.024)$  MeV/c<sup>2</sup> [5]. Experiments in which the  $\eta$  meson was identified through a missing-mass peak in a hadronic production reaction have all reported a lower value for the mass, typically by about 0.5 MeV/c<sup>2</sup>. This was the case for the  $\pi^-p \rightarrow n\eta$  reaction, where the beam momentum was determined macroscopically to high precision using the floating wire technique [6]. In the two experiments where the  $dp(pd) \rightarrow {}^3\text{He}\eta$  reaction was used [7, 8], the beam momentum was measured by study-

ing other two-body reactions with known final masses. One possible concern might be whether the background under the  $\eta$  peak could have been slightly distorted by a strong coupling of, for example,  $\eta {}^3\text{He} \rightleftharpoons \pi\pi {}^3\text{He}$ . Alternatively, the beam momenta could have been poorly determined, though this was done using different techniques for the three experiments [6–8], or the spectrometers aligned insufficiently well.

The situation can only be clarified through the performance of a much more precise missing-mass experiment [20]. It is the purpose of the present paper to provide results of such an investigation of the two-body  $dp \rightarrow {}^3\text{He}\eta$  reaction near threshold that is comparable in accuracy with those that studied the  $\eta$  decay products [1–4]. For this to be successfully achieved, it is necessary (i) to establish the beam momentum, (ii) to identify well the  $\eta$  meson from the  $dp \rightarrow {}^3\text{He}X$  missing-mass peak, and (iii) to establish the increase of the final-state momentum with excess energy  $Q = \sqrt{s} - (m_{{}^3\text{He}} - m_\eta)c^2$  above the  ${}^3\text{He}\eta$  reaction threshold with high accuracy. Here  $\sqrt{s}$  is the total center-of-mass (c.m.) energy. A data set of beam momenta and associated final-state momenta near threshold then permits the determination of the production threshold and hence the  $\eta$  meson mass.

In order to obtain a clean identification of the  $\eta$  meson from a missing-mass peak in a  $dp \rightarrow {}^3\text{He}X$  reac-

\*Electronic address: paul.goslawski@uni-muenster.de

†Electronic address: khoukaz@uni-muenster.de

tion, it is important that  $\eta$  production be very strong in the near-threshold region. Here we are particularly fortunate in that the  $dp \rightarrow {}^3\text{He}\eta$  total cross section rises within the first 1 MeV above threshold to its plateau value of  $\approx 400$  nb and then remains nearly constant up to  $Q = 100$  MeV [9, 10]. This allows one to collect similar statistics over a wide excess energy range, even very close to threshold, without expending excessive measuring time. Furthermore, it has been demonstrated that the ANKE facility is well suited for measuring the total and differential cross sections of the  $dp \rightarrow {}^3\text{He}\eta$  reaction. The spectrometer has full geometrical acceptance for excess energies  $Q < 15$  MeV. The multipion background under the  $\eta$  peak varies smoothly with  $Q$ , making a robust subtraction of this background possible [9, 10].

The extrapolation of data to identify the production threshold requires a precise measurement of the increase of the  ${}^3\text{He}$  c.m. momentum as a function of the beam momentum. Due to resolution or smearing effects, which are always present in any real detector, the reconstructed momenta can be shifted compared to the true ones. To understand and compensate for such effects, a careful study of the entire ANKE spectrometer is needed. After calibrating the spectrometer by measuring a variety of other nuclear reactions, the requisite precision was achieved by demanding that the magnitude of the true  ${}^3\text{He}$  momentum from the  $dp \rightarrow {}^3\text{He}\eta$  reaction should be identical in all directions in the c.m. frame. This check was only possible because of the 100% angular acceptance of ANKE for the reaction of interest.

We have previously described in full the measurement of the beam momenta via the induced spin depolarization technique [11]. The background subtraction that allows the extraction of the  $\eta$  meson signal from the  $dp \rightarrow {}^3\text{He}X$  reaction is essentially identical to that of our earlier work [9]. Therefore, most of the emphasis here will be on describing the fine calibrations of the spectrometer required to get the necessary precision in the final  ${}^3\text{He}$  momenta. After outlining the method for determining the  $\eta$  mass in Sec. II, the beam momentum determination is briefly summarized in Sec. III. The standard calibration of the ANKE forward detector system is given in Sec. IV. Section V discusses how to exploit the full geometrical acceptance of a two-body reaction, such as  $dp \rightarrow {}^3\text{He}\eta$ , to verify and improve the alignment of the spectrometer. Results and estimated uncertainties are presented and it is shown how resolution effects can influence the measurement of the final-state momenta and hence the missing mass.

The results of the determinations of the beam and final-state momenta are brought together in Sec. VI so that a reliable extrapolation to the  $\eta$  threshold can be made. In this way, a value for the mass of the  $\eta$  meson was obtained with small systematic and negligible statistical errors. The comparison with the results of other experiments is made in our conclusions of Sec. VII. The good agreement with other precision measurements was only achieved through the exploitation of the large angu-

lar acceptance of ANKE for this  $\eta$ -production reaction, a feature that was not available in earlier missing-mass experiments.

## II. METHOD FOR THE DETERMINATION OF THE $\eta$ MESON MASS

By studying the two-body  $dp \rightarrow {}^3\text{He}\eta$  reaction in a fixed-target experiment, the  $\eta$  mass can be determined by measuring only the momenta of the deuteron beam and the recoiling  ${}^3\text{He}$ . In a standard missing-mass experiment, the  $\eta$  mass is extracted by measuring the relevant kinematic variables at a single fixed energy. This requires both a precise calibration of the detector, for a correct determination of the  ${}^3\text{He}$  momentum, and an accurate measurement of the deuteron beam momentum.

A much more effective way to measure the  $\eta$  mass relies on the determination of the production threshold by investigating the change of the final-state momentum as a function of the beam momentum. This requires the kinematics to be measured at several different energies close to threshold. For the  $dp \rightarrow {}^3\text{He}\eta$  reaction, the final-state momentum  $p_f$  in the c.m. frame

$$p_f(s) = \frac{\sqrt{[s - (m_{{}^3\text{He}} + m_\eta)^2][s - (m_{{}^3\text{He}} - m_\eta)^2]}}{2\sqrt{s}}, \quad (1)$$

is a very sensitive function of the  $\eta$  mass and the total energy  $\sqrt{s}$ . The latter is completely fixed by the masses of the initial particles and the laboratory momentum,  $p_d$ , of the deuteron beam;

$$s = 2m_p\sqrt{m_d^2 + p_d^2} + m_d^2 + m_p^2. \quad (2)$$

The final-state momentum depends only on the beam momentum, the  $\eta$  mass and other well-measured masses [12]. If one can fix the production threshold,  $p_f(s) = 0$ , the  $\eta$  mass can then be determined from knowledge of  $p_d$ . The precision is enhanced because in this region  $dm_\eta/dp_d \approx 0.24/c$ .

An obvious advantage of the threshold determination method is that it does not require a perfect spectrometer calibration. This is illustrated in Fig. 1 using Monte Carlo simulated data at twelve different excess energies in the range of  $Q = 1 - 11$  MeV and assuming some fixed value of the  $\eta$  mass. Although the analysis was performed using Eq. (1) (solid line), to first order  $p_f^2$  depends linearly on  $p_d$  near threshold.

To reduce the sensitivity of the method to systematic errors in the spectrometer calibration, an additional scaling factor  $S$  is introduced which multiplies the right-hand side of Eq. (1). Such a factor will occur in a real experiment, e.g., through minor inaccuracies in the determination of the interaction vertex relative to the detection system. If one then used data at a single excess energy, this would lead to an error in the determination of the

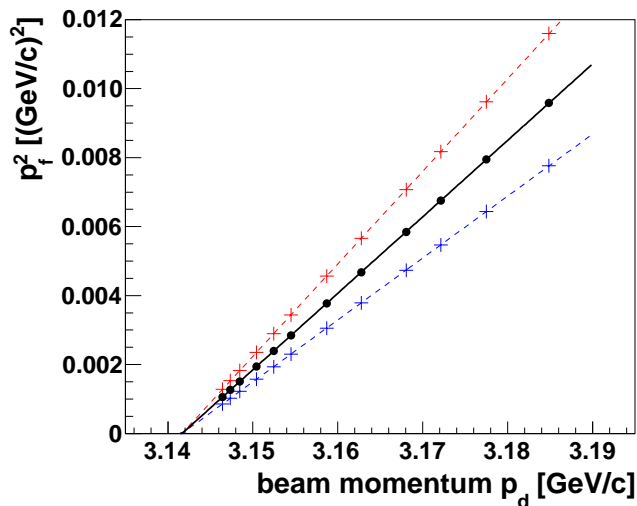


FIG. 1: (color online) Identification of the  $dp \rightarrow {}^3\text{He}\eta$  production threshold by studying the relationship between the square of the final-state momentum  $p_f$  and the deuteron beam momentum  $p_d$ . The twelve Monte Carlo points are compared with the shape expected from the kinematics (solid line). Although this shape depends slightly on  $m_\eta$ , it is essentially a straight line over the range shown. The stability of the threshold extrapolation is illustrated by the dashed red and blue lines, where the measurements of  $p_f$  are scaled by arbitrary constants  $S = 0.9$  and  $1.1$ , respectively.

missing mass. However, by measuring over a range of excess energies, such a scaling factor would not affect the value of  $p_d$  corresponding to the production threshold that is used in the mass determination. This effect is illustrated by the dashed lines in Fig. 1, where 10% changes in the scaling factor were considered.

### III. BEAM MOMENTUM DETERMINATION

A method to determine the beam momentum to high precision in a storage ring was developed at the electron-positron machine VEPP-2M at Novosibirsk [13]. The technique uses the spin dynamics of a polarized beam and relies on the fact that depolarizing resonances occur at well-defined frequencies, which, apart from the gyromagnetic anomaly, depend only upon a particle's speed. By depolarizing a polarized beam with an artificial spin resonance induced by a horizontal radio frequency magnetic field of a solenoid, the value of the beam momentum can be measured to high accuracy. The frequency of such an artificial resonance  $f_r$  is fixed in terms of the machine frequency  $f_0$  by the relativistic  $\gamma$  factor of the particle. Since frequencies can be routinely measured with a relative precision  $\approx 10^{-5}$ , an accurate value of  $\gamma$  and hence momentum can be deduced. When this method was used for the first time at COSY with a vector-polarized deuteron beam, the precision achieved was more than an order of magnitude better than that of conventional methods [11].

In the COSY-ANKE experiment, twelve closely-spaced beam momenta above the  $dp \rightarrow {}^3\text{He}\eta$  threshold were divided alternately into two so-called supercycles that involved up to seven different machine settings. In addition to six momenta above threshold, one was included below threshold in both supercycles to provide the background description. Each supercycle covered an excess energy range from  $\approx 1$  MeV to  $\approx 10$  MeV. The beam momenta were measured both before and after five days of data-taking in order to study systematic effects.

In both supercycles there were collective shifts of the spin resonance frequencies of  $\approx 12 - 17$  Hz, which probably originated from changes in the orbit length in COSY of about 3 mm. The set of beam momenta from the first supercycle were found to decrease slightly over the data-taking time whereas those of the second supercycle showed the inverse behavior. Average values of the measurements, before and after data-taking, were calculated for each of the twelve beam momenta and these were used in the threshold fits. The maximum uncertainty for these mean values was conservatively evaluated as  $\pm 164$  keV/c. It is reasonable to assume that the orbits changed linearly in time to give a uniform probability distribution of true momenta over this interval. The systematic uncertainty of the averaged beam momenta is therefore estimated to be  $\Delta p_{d,\text{sys}} = 95$  keV/c (rms). Evidence in favor of the approach adopted here is found by comparing the results obtained with the two supercycles, which are discussed in Sec. VI.

The statistical uncertainty in one of the twelve beam momenta in the range 3.1–3.2 GeV/c is dominated by that of the revolution frequency  $f_0$ . The measured revolution frequency deviated randomly by up to  $\pm 6$  Hz from measurement to measurement. The rms uncertainty in this frequency, 3.5 Hz, corresponds to a statistical uncertainty in the beam momentum of  $\Delta p_{d,\text{stat}} = 29$  keV/c.

In total, the twelve beam momenta were measured with an overall accuracy of  $\Delta p_d/p_d = 3 \times 10^{-5}$ . This is sufficient to satisfy the needs of a competitive  $\eta$  mass measurement.

## IV. THE ANKE SETUP

### A. The ANKE magnetic spectrometer

The experiment was performed at the Cooler-Synchrotron of the Forschungszentrum Jülich [14] using the ANKE magnetic spectrometer [15] that is located at an internal target station of the storage ring. ANKE includes three dipole magnets (D1, D2, D3) that deflect the COSY beam through a chicane in the ring (see Fig. 2). This allows particles produced at small angles, which would normally escape down the beam pipe, to be detected and this is of particular importance for near-threshold reactions. D1 deflects the circulating beam by an angle off its straight path onto a cluster-jet target [16], the spectrometer dipole magnet D2 separates the

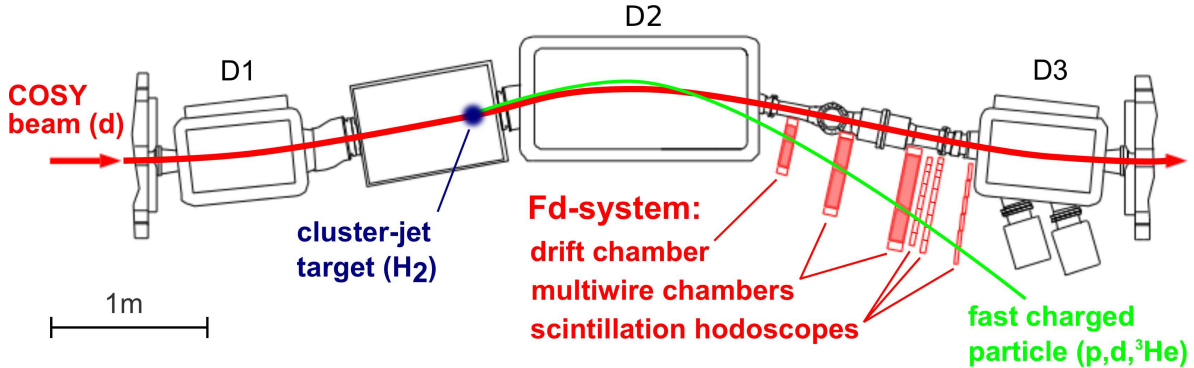


FIG. 2: (color online) The ANKE setup used for the determination of the  $\eta$  mass. The COSY deuteron beam hits the hydrogen cluster-jet target and the charged particles produced at small angles are separated by the D2 spectrometer magnet to be detected by the ANKE Fd-system.

produced particles from the beam for momentum analysis, and D3 leads the unscattered particles back onto the nominal orbit. Although ANKE is equipped with a variety of detectors, only the Forward system (Fd) was used for the  $\eta$  mass measurement. This consists of one drift chamber, two multiwire proportional chambers, and three layers of scintillation hodoscopes [17, 18]. The location of the various elements of the experimental setup is illustrated in Fig. 2.

The design requires the D2 magnet and the forward system to be placed jointly on a moveable platform. The deflection angle of the beam,  $\alpha$ , depends on the position of the platform. The angle ( $0^\circ \leq \alpha \leq 10.6^\circ$ ), the magnetic field strength of D2 ( $\leq 1.57$  T), and the beam momentum cannot be chosen independently of each other. By adjusting these three parameters it is possible to increase the geometrical acceptance. The deflection angle, which may differ slightly from the nominal one, was determined to be  $5.8^\circ$ .

The tracks of fast charged particles detected in the ANKE Fd-system can be traced back through the precisely known magnetic field to the interaction point and this leads to a momentum reconstruction for registered particles.

### B. The standard Fd-system calibration

In addition to the three parameters mentioned, i.e., the magnetic field, deflection angle, and interaction point, the drift and wire chamber positions also have to be determined with high accuracy, and this requires a precise calibration of the detection system. In the standard procedure [19], the positions of the drift and wire chambers on the movable platform are first aligned by using data taken at the beginning of the beam time with a deflection angle of  $0^\circ$  and no magnetic field in D2. The ejectiles then move on straight tracks starting from the nominal interaction point in the overlap region of the COSY beam and

the cluster-jet target. From an analysis of these tracks, the position of the Fd-detector relative to the D2 magnet and the target can be reconstructed and compared to direct measurements.

After making this first alignment, the global positions of the drift and wire chambers are defined by that of the moveable Fd-system platform. Although the positions of the platform and interaction vertex are already known by direct measurement, a much more precise determination of their values is possible by investigating a series of reference reactions at all the energies used in the  $\eta$ -mass determination. These are:

1. Small angle  $dp \rightarrow dp$  elastic scattering, with the fast forward deuteron being detected,
2. Large angle  $dp \rightarrow dp$  elastic scattering, with both final-state particles being detected,
3.  $dp \rightarrow ppn$  charge-exchange, with two fast protons being detected, and
4.  $dp \rightarrow {}^3\text{He} \pi^0$ , with the  ${}^3\text{He}$  nucleus being detected.

Deuteron-proton elastic scattering in the backward hemisphere allows one to verify energy-momentum conservation in the reconstructed four-momenta. For the other reactions, the minimization of the deviation of the missing mass from the expected value was used to fix the positions of the interaction vertex and the Fd-system platform. With the parameters extracted at thirteen different beam energies, the missing masses were reconstructed to an accuracy of  $\approx 3$  MeV/ $c^2$  for all four channels studied. Though good, it is manifestly insufficient for a competitive determination of the  $\eta$  mass and the more refined technique discussed in the following section is needed.

## V. THE ${}^3\text{He}\eta$ FINAL-STATE MOMENTUM ANALYSIS

### A. Fine calibration using the kinematics of the $dp \rightarrow {}^3\text{He}\eta$ reaction

The calibration method described in Sec. IV B, i.e., the study of kinematic variables in measured reactions with known masses, is standard for magnetic spectrometers and was used in such a way in other  $\eta$  missing-mass experiments [7, 8]. Unlike these experiments, the ANKE facility has full geometrical acceptance for the  ${}^3\text{He}$  from the  $dp \rightarrow {}^3\text{He}\eta$  reaction up to an excess energy  $Q \approx 15$  MeV. By taking advantage of this feature and studying the dependence of the final-state momentum on the  ${}^3\text{He}$  c.m. angles, the standard calibration could be significantly improved.

For a two-body reaction at a fixed center-of-mass energy, the final-state momenta  $p_f$  are distributed on a sphere in the c.m. frame with a constant radius given by Eq. (1). We take the  $z$ -direction to lie along that of the beam,  $y$  to be defined by the upward normal to the COSY ring, and  $\hat{x} = \hat{y} \times \hat{z}$ . The relation of Eq. (1) can be visualized in a simplified way by plotting the magnitude of the transverse momentum,  $p_\perp = \sqrt{p_x^2 + p_y^2}$ , versus the longitudinal momentum  $p_z$  for reconstructed events, as shown in Fig. 3. For a better visualization of the angular distribution, each event is weighted with a factor  $1/p_\perp$ . The expected kinematic loci for  $dp \rightarrow {}^3\text{He}\eta$  and  $dp \rightarrow {}^3\text{He}\pi^0$  are shown by solid lines. It is clear that the numbers of events vary along the circles but the method used here only depends upon the position of a kinematic curve and not on its population. In addition to single meson production, there is a large accumulation of events near the forward direction for  $p_f \approx 350$  MeV/ $c$  and these correspond to two-pion production in the  $dp \rightarrow {}^3\text{He}(\pi\pi)^0$  reaction.

The principle of the refined spectrometer calibration is the requirement that the momentum sphere should be completely symmetric in  $p_x$ ,  $p_y$ , and  $p_z$ . It is therefore necessary to study the reconstructed momentum  $p_f$  carefully as a function of the polar and azimuthal angles  $\vartheta$  and  $\phi$ . This requires a clean separation of the  ${}^3\text{He}\eta$  signal from the background and this is the first step in the analysis.

In the event selection,  ${}^3\text{He}$  particles were identified and the raw background, consisting mainly of deuterons and protons from  $dp$  elastic scattering and protons from deuteron breakup, was suppressed by cuts on the energy loss and time of flight of charged particles in the Fd detector. Figure 4(a) shows the energy loss times the square of the particle velocity versus the laboratory momentum. A projection of these events onto the ordinate gives a clear peak with a low background. In our analysis we used a very loose cut at the  $6\sigma$  level but, as will be shown in Sec. VI, changing this to  $3\sigma$  would have only a tiny effect on the value obtained for  $m_\eta$ .

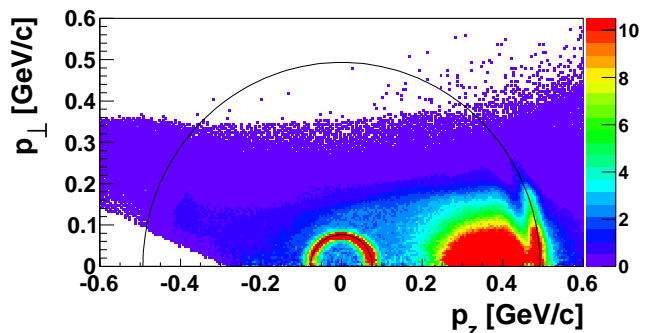


FIG. 3: (color online) The magnitude of the reconstructed transverse c.m. momentum  $p_\perp$  in the  $dp \rightarrow {}^3\text{He}X$  reaction plotted against the longitudinal c.m. component  $p_z$  at an excess energy  $Q = 6.3$  MeV with respect to the  $\eta$  threshold. For better visualization of the angular distribution, each event is weighted with a factor  $1/p_\perp$ . The small and large circles correspond to the kinematic loci for the  $dp \rightarrow {}^3\text{He}\eta$  and  $dp \rightarrow {}^3\text{He}\pi^0$  reactions, respectively. ANKE covers the full solid angle for  $\eta$  production near threshold whereas, for pions, only the forward  ${}^3\text{He}$  are detected.

Figure 4(b) shows a typical example for one scintillation counter combination of the length of the reconstructed flight path of the  ${}^3\text{He}$  selected from the events in Fig. 4(a). This has been calculated from the TOF information between the first and the last scintillation wall in the forward detector and the reconstructed particle momentum, assuming the mass and charge of the  ${}^3\text{He}$ . A clear peak is again evident with only a moderate background. Reducing the  $3\sigma$  cut used here to  $2\sigma$  gives an even smaller change in the value of  $m_\eta$ .

The remaining background, shown in Figs. 3 and 5, originates mainly from some residual deuteron breakup and multipion production in the  $dp \rightarrow {}^3\text{He}X$  reaction, where  $X = (\pi\pi)^0$  or  $X = (\pi\pi\pi)^0$ . At the lowest excess energy, the signal/background ratio is around 11 but this decreases with increasing excess energy to  $\approx 1.8$  at  $Q = 10.4$  MeV. This background was subtracted using the data taken below the  $\eta$  threshold at an excess energy of  $Q \approx -5$  MeV. These data were kinematically transformed to positive  $Q$  in order to compare them with results obtained above threshold. The details of this technique are described for missing-mass spectra in Ref. [9], but the method is equally applicable to final-state momentum spectra. Due to the very high statistics of the current experiment, the distribution in  $p_f$  could be investigated for twenty bins each in  $\vartheta$  and  $\phi$ . This is illustrated in Fig. 5, where examples of the  $p_f$  spectra summed over  $\phi$  are shown for six  $\cos\vartheta$  bins for the energy closest to threshold,  $Q = 1.1$  MeV. A similar picture is found for the  $\phi$  dependence after summing over  $\theta$ .

Mean values of the  ${}^3\text{He}$  momentum  $p_f$  and the peak widths for different  $\vartheta$  and  $\phi$  bins were extracted from the background-subtracted  $dp \rightarrow {}^3\text{He}\eta$  distributions by making Gaussian fits. A variation of the width of 4–12 MeV/ $c$  (rms) was found, as well as a displacement of

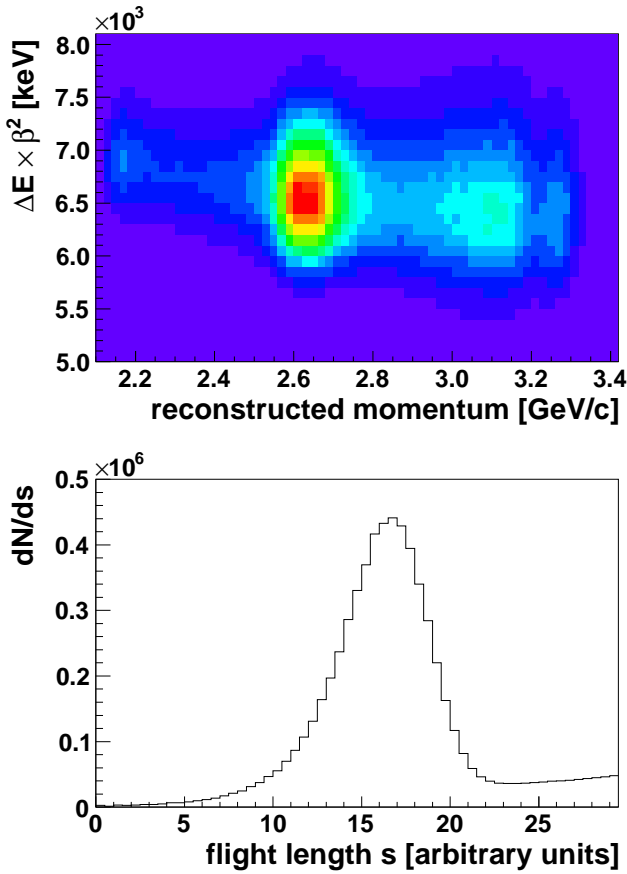


FIG. 4: (color online) (a) Two-dimensional distribution of energy loss times the square of the particle velocity versus its laboratory momentum. A projection of this onto the  $y$ -axis gives a peak with little background. Data within a  $\pm 6\sigma$  cut were retained for further analysis. (b) A typical flight length distribution for events selected from panel (a). Data within a  $\pm 3\sigma$  range were used in the subsequent analysis.

the mean value, both of which depended upon the polar and azimuthal angles. This striking effect results from the different resolutions of the ANKE Fd-system in  $p_x$ ,  $p_y$  and  $p_z$ , which are discussed in the following section.

### B. Influence of the momentum resolution on the reconstructed final-state momentum

The influence of resolution on the angular dependence of the reconstructed  ${}^3\text{He}$  momentum and the missing-mass distributions for the  $dp \rightarrow {}^3\text{He}\eta$  reaction is illustrated by the two-dimensional  $(p_\perp, p_z)$  projection shown in Fig. 6(a). In the ideal case of a measurement with perfect resolution, the final-state momenta are distributed on a sphere of constant radius  $p_f$ , as indicated by the black line. Both the missing mass and final-state momentum are then independent of  $\cos\vartheta$  and  $\phi$ , as illustrated by the black line in Figs. 6(b)-6(e).

In a real experiment, the reconstructed momenta in

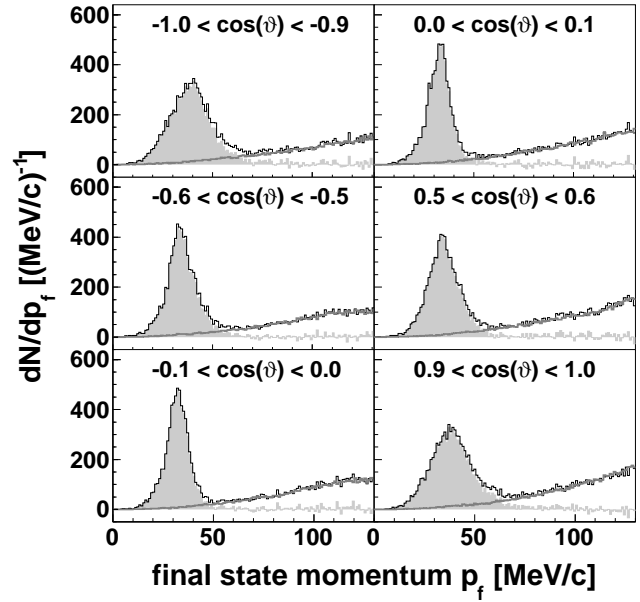


FIG. 5: Center-of-mass distributions of the  ${}^3\text{He}$  momentum from the  $dp \rightarrow {}^3\text{He}X$  reaction for six typical polar angle bins at the lowest excess energy measured,  $Q = 1.1$  MeV. The experimental data summed over  $\phi$  are shown by black lines and the background estimated from subthreshold data by gray lines. The resulting background-subtracted  $dp \rightarrow {}^3\text{He}\eta$  signal is shaded gray.

the laboratory frame are smeared by the finite resolution associated with the detector setup and reconstruction algorithms. If only  $p_z$  were smeared, with a Gaussian width of say  $\sigma_z = 30$  MeV/c in the laboratory frame, an event on the momentum sphere, indicated by the black arrow in Fig. 6(a), could be shifted along the red arrows. It is important to note that for  $p_f^{\text{rec}} < p_f^{\text{true}}$  events are shifted toward lower  $|\cos\vartheta|$  whereas the reverse is true for  $p_f^{\text{rec}} > p_f^{\text{true}}$ . This effect leads to a  $p_f$  distribution that is a function of  $\cos\vartheta$  (Fig. 6(b), red circles), i.e., the momentum sphere is stretched for large longitudinal momenta and compressed for high transverse momenta. For simple kinematic reasons, the missing mass shows the inverse behavior [see Fig. 6(d)]. Since the smearing was here assumed to be independent of  $p_x$  and  $p_y$ , and hence  $\phi$ , this is reflected in the constancy of the reconstructed momentum in Fig 6(c). Nevertheless, its value is higher than the true one,  $p_f^{\text{rec}}$ .

When only the transverse momenta are smeared, but with different Gaussian widths, e.g.,  $(\sigma_x, \sigma_y, \sigma_z) = (10, 20, 0)$  MeV/c, the reconstructed momentum has the opposite dependence on  $\cos\vartheta$ . As shown by the blue crosses in Fig. 6(b),  $p_f$  decreases for  $\cos\vartheta \approx \pm 1$  and increases for  $\cos\vartheta \approx 0$ . Different resolutions in  $p_x$  and  $p_y$  also introduce a dependence on  $\phi$ , and this leads to oscillations in both  $p_f^{\text{rec}}$  and the missing mass in the plots of Figs. 6(c) and 6(e). The amplitude and phase of these oscillations depend on the ratio  $\sigma_x/\sigma_y$ .

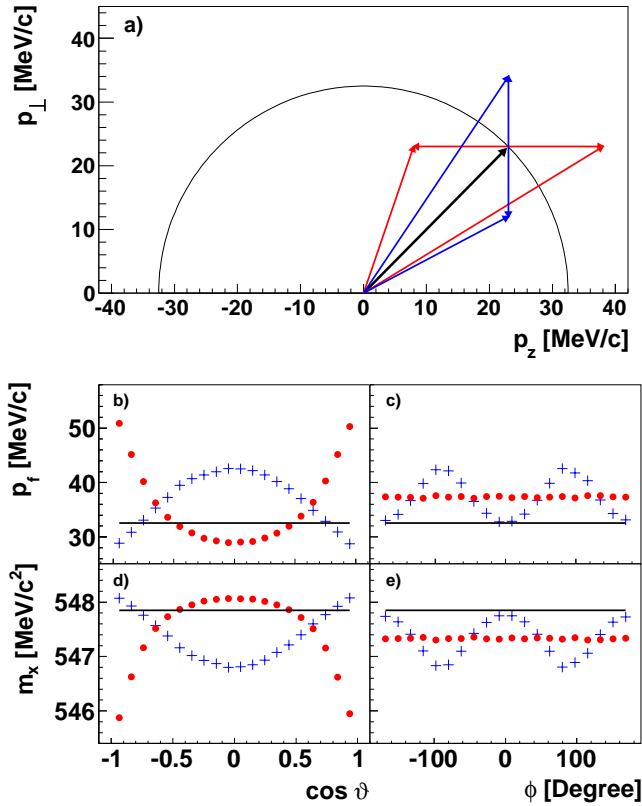


FIG. 6: (color online) Influence of resolution on the determination of the final-state momentum. The ideal  $p_f$  sphere of panel (a) (black) is changed along the horizontal (red) arrow by finite resolution in the longitudinal ( $z$ ) direction, whereas resolution effects in the transverse direction are indicated by the vertical (blue) arrow. Panels (b) – (e) show the possible distortions at  $Q = 1.1$  MeV, evaluated in Monte Carlo simulation. The mean values of both the final-state momentum and the missing-mass distributions for individual  $\cos\vartheta$  and  $\phi$  bins are shown without (black line) and with momentum smearing in the  $z$ -direction (red circles) and transversely (blue crosses).

In reality, all three momentum components are reconstructed with finite and generally different resolutions and the effects described above will be superimposed, though they will be dominated by the component with the worst resolution. The determination of the  $\eta$  mass has to take these kinematic resolution effects into account because, without so doing, the value extracted for  $m_\eta$  would depend on the production angle. For the current ANKE experiment, differences in  $m_\eta$  of up to  $0.5$  MeV/ $c^2$  are found between  $\cos\vartheta = \pm 1$  and  $\cos\vartheta = 0$ . Furthermore, the average of the final-state momentum over all  $\cos\vartheta$  and  $\phi$  is shifted to a higher value than the true one and the missing mass shifted to a lower value. The angular distribution of the  $dp \rightarrow {}^3\text{He}\eta$  reaction could modify slightly the effects of the resolution but, since this variation is linear in  $\cos\vartheta$  over all the  $Q$ -range studied [9], even this is of little consequence for the determination of  $m_\eta$ , given the symmetry in  $\cos\vartheta$  shown in Fig. 6(b).

Precise determinations of the resolutions in  $(p_x, p_y, p_z)$  are absolutely essential in order to correct the measured kinematic variables. How this is done, by demanding an isotropic  $p_f$  momentum sphere, will be discussed next in some detail in Sec. V C.

### C. Correction to the final-state momenta

Mean values of the measured final-state momenta for background-subtracted  $dp \rightarrow {}^3\text{He}\eta$  distributions are shown in Fig. 7 for twenty individual  $\cos\vartheta$  and  $\phi$  bins at an excess energy  $Q = 1.1$  MeV, before and after the improvement of the calibration. The results for the standard calibration, presented in the upper panels, show that the momentum sphere is neither centered nor symmetric. The momentum sphere is shifted to higher  $p_z$ , i.e., on average  $p_f$  is higher for  ${}^3\text{He}$  produced in the forward direction than in the backward. The oscillations in the  $\phi$  spectrum are also far from being symmetric, and this is particularly evident at  $\phi \approx \pm 90^\circ$ , where the  $p_y$  momentum component dominates. This asymmetric pattern is rather similar at all twelve energies and this stresses the need to improve the calibration for the determination of the correct momenta.

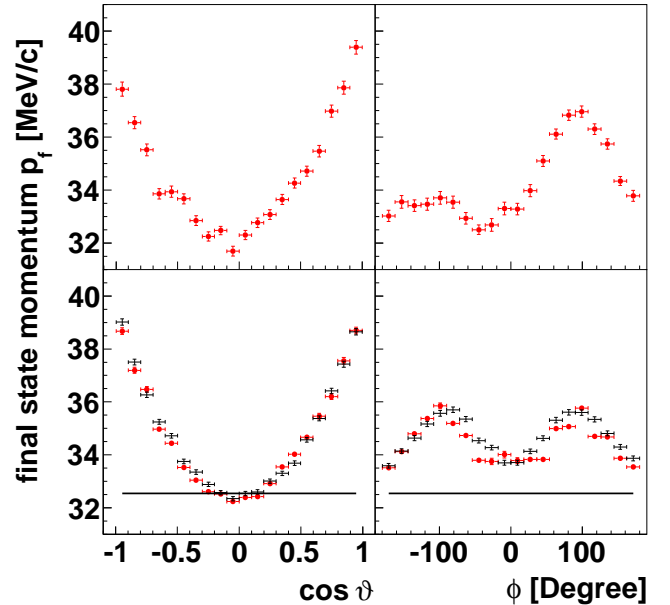


FIG. 7: (color online) The mean values of the final-state momentum distributions are shown for individual  $\cos\vartheta$  and  $\phi$  bins for the standard (top) and improved (bottom) calibration at  $Q = 1.1$  MeV (red circles). The results of Monte Carlo simulations are shown without (black horizontal line) and with momentum smearing (black points). The comparison of the data with the simulation leads to a determination of the momentum resolutions in the three directions.

The  $p_y$  component depends sensitively on the relative  $y$ -position between the two wire chambers in the forward

detector and, by varying their positions by about 0.3 mm, the momentum sphere could be centered in  $p_y$ . Changes in the magnetic field strength of 0.0015 T at 1.4 T, i.e., changes of the order of 0.1%, allow one to make the necessary adjustment in the  $p_z$  component. The  $p_x$  component can be fine-tuned by adjusting the deflection angle  $\alpha$  by about 0.4% at  $5.8^\circ$ . By making changes such that the mean values of the final-state momenta are distributed on a centered and perfectly symmetric sphere in  $\cos\vartheta$  and  $\phi$ , the detector alignment can be significantly improved, as shown in the lower part of Fig. 7. This procedure was carried out using the data at all twelve energies simultaneously. The magnitudes of these changes are so small that they have no impact on the values of the missing masses of the different reactions used in the standard calibration.

The improved spectra, shown in the lower half of Fig. 7 for one of the twelve energies, allow one to study the momentum smearing in the three directions. The values of  $\sigma_x$  and  $\sigma_y$  were determined from the amplitude and phase of the oscillation in  $\phi$ , as explained in Sec. VB, whereas that of  $\sigma_z$  was extracted by making a second order fit to the data and simulations for  $p_f$  as a function of  $\cos\vartheta$ . An additional constraint is that the values of  $(\sigma_x, \sigma_y, \sigma_z)$  must reproduce the width of the  ${}^3\text{He}\eta$  final-state momentum signal when integrated over all  $\vartheta$  and  $\phi$ . The resolution parameters were determined from the spectra with uncertainties of  $(\Delta\sigma_x, \Delta\sigma_y, \Delta\sigma_z) = (0.2, 0.2, 0.1)$  MeV/c.

The individual momentum spreads were determined separately for each of the twelve energies. In contrast to  $\sigma_z$ , which is constant to within 1 MeV/c,  $\sigma_x$  decreases and  $\sigma_y$  increases with excess energy. This behavior is reasonable because the cone angle of the  ${}^3\text{He}$  ejectiles from the  $dp \rightarrow {}^3\text{He}\eta$  reaction increases with excess energy. Close to threshold the hit positions in the chambers are located in a small area near the center of the wire chambers, whereas at higher  $Q$  the hits are more widely distributed. With the resolution parameters thus determined, data similar to those shown in Fig. 7 are described well by Monte Carlo simulations at all twelve energies. Figure 8 shows the distribution of the final-state momentum summed over all  $\cos\vartheta$  and  $\phi$  at an excess energy of  $Q \approx 8.6$  MeV. It is clear that the measured momentum distribution (filled area) is generally very well reproduced by the Monte Carlo simulated data (black crosses).

Using data from all twelve energies above threshold, a mean momentum resolution of ANKE was calculated in the narrow  ${}^3\text{He}$  laboratory momentum range of 2.63–2.68 GeV/c. The values of the momentum spreads in the laboratory frame were found to be  $(\sigma_x, \sigma_y, \sigma_z) = (2.8, 7.9, 16.4)$  MeV/c. As expected for a fixed target experiment, the resolution in  $p_z$  is by far the poorest. Furthermore, because of the particular construction of the wire chambers, the  $p_x$  resolution is better than that for  $p_y$ . However, in the determination of the final-state momentum corrections, the individual resolution param-

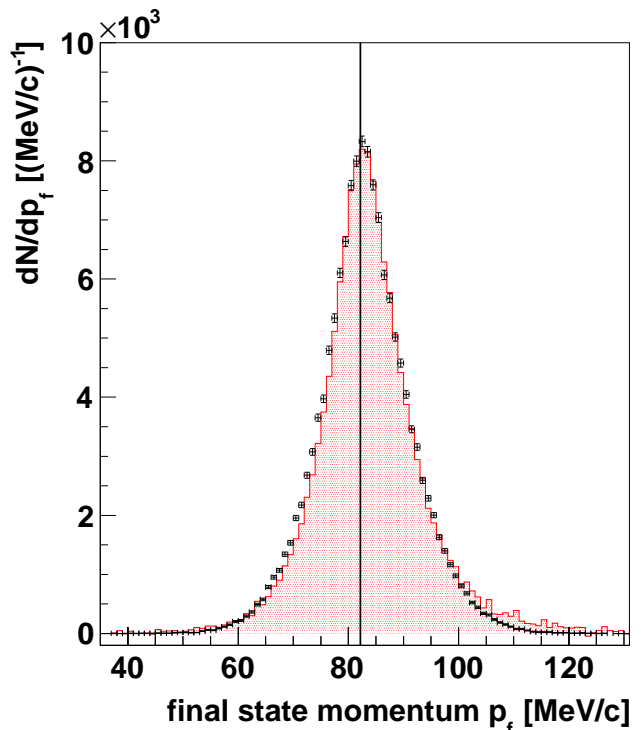


FIG. 8: (color online) Final state momentum distribution for background-subtracted  $dp \rightarrow {}^3\text{He}\eta$  data (filled red area) and simulation (black crosses) for all events at an excess energy of  $Q \approx 8.6$  MeV. The vertical line indicates the true final-state momentum assumed in the simulation.

eters determined at each beam momentum were used.

Owing to the resolution effects shown in the lower half of Fig. 7, the average of the final-state momentum over all  $\cos\vartheta$  and  $\phi$  is shifted to a higher value than the true one (black horizontal line). By comparing the averages resulting from the Monte Carlo simulations with and without momentum smearing, correction parameters were calculated for all twelve energies and these are presented in Fig. 9. The correction is about 2.22 MeV/c for the lowest momentum and decreases steadily with  $p_f$ . The error bars shown are dominated by the uncertainties in the resolution parameters  $(\Delta\sigma_x, \Delta\sigma_y, \Delta\sigma_z)$  and range from 0.08 MeV/c at the lowest beam momentum to 0.04 MeV/c at higher energies. It should be noted that the dependence of the correction parameters on the value assumed for the  $\eta$  mass is negligible.

If the resolution factors  $\sigma_i$  are largely independent of the beam momentum, the correction should vary like  $\sim 1/p_f$ . This behavior arises because the deviation depends on the ratio of the ANKE momentum resolution to the size of the momentum sphere. Confirmation of such a dependence is offered by the curve, which is a  $1/p_f$  fit to the data. Despite the good  $\chi^2/\text{NDF} \approx 0.9$ , the individual Monte Carlo estimates were used in the subsequent analysis.

Compensation for the effects of the momentum res-

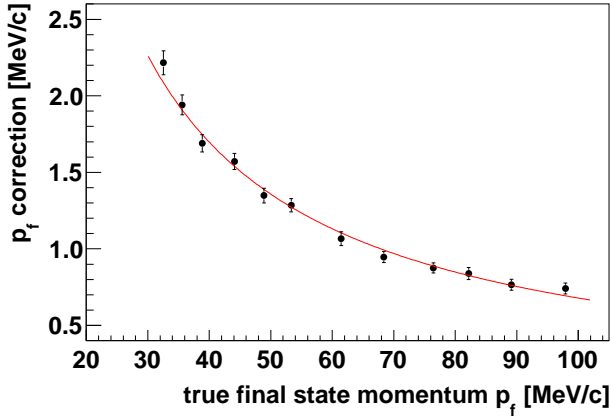


FIG. 9: (color online) Deviation of the measured final-state momentum in the  $dp \rightarrow {}^3\text{He}\eta$  reaction from the true one due to resolution effects, evaluated in Monte Carlo simulation. The twelve measured final-state momenta in the near-threshold region,  $Q = 1\text{--}11$  MeV, have to be corrected by 0.7–2.2 MeV/ $c$  to compensate for such effects. The curve is a  $1/p_f$  fit to the points.

olution is essential for an accurate determination of the production threshold. Without this correction, the value obtained for the  $\eta$  mass would be lower by about 150 keV/ $c^2$ .

## VI. THE MASS OF THE $\eta$ MESON

In order to obtain a robust value for the mass of the  $\eta$  meson, it is necessary to extrapolate the experimental data with high precision in order to determine the value of the deuteron beam momentum at threshold. For this purpose we show the complete set of final-state and beam momenta ( $p_f, p_d$ ) with statistical uncertainties in Table I. Also shown are the corrections that were included in the values quoted for  $p_f$ .

Due to the resolution effects, the twelve  $p_f$  distributions are found to be slightly asymmetric over the whole angular range, both for the experimental data as well as the Monte Carlo simulated events, as shown for a typical energy in Fig. 8. The values of the  $p_f$  means were determined for both data and simulations within  $\pm 3\sigma$  limits. The good statistics of  $\approx 1.3 \times 10^5$   ${}^3\text{He}\eta$  events for each energy meant that the uncorrected value for  $p_f$  could be extracted with an uncertainty of  $\approx 23$  keV/ $c$ . In total  $\approx 1.5 \times 10^6$   ${}^3\text{He}\eta$  events were collected in the experiment. After applying the resolution correction to the measured  $p_f$ , the overall uncertainty is increased, as indicated in Table I.

Although the description of the reconstructed final-state momentum distribution in Fig. 8 by the Monte Carlo simulation is very good, it is not perfect, especially in the high momentum tail. Such discrepancies could arise from slight imperfections in the spectrometer

calibration,  ${}^3\text{He}$  scattering in the wire chambers, or limitations in the background subtraction approach. In order to quantify their influence on the value extracted for the  $\eta$  mass, the interval used to determine the means of the  $p_f$  was varied between  $\pm 2\sigma$  to  $\pm 4\sigma$ , where  $\sigma$  represents the peak width. Such a variation leads to a collective shift in the extracted final-state momenta of approximately 0.16 MeV/ $c$ . Since this effect corresponds to an overall shift in the final state momenta, it is not included in the numbers quoted in Table I but must be considered in the final  $\eta$  mass determination, where it introduces a systematic uncertainty of 12 keV/ $c^2$ .

TABLE I: Values of the laboratory beam momenta  $p_d$ , corrected final-state c.m. momenta  $p_f$ , and the  $p_f$  correction parameters measured at twelve different excess energies; the statistical uncertainties are noted in brackets. The approximate values of  $Q$  quoted here are merely used to label the twelve settings.

Excess energy $Q$ MeV	Beam momentum $p_d$ MeV/ $c$	Final-state momentum $p_f$ MeV/ $c$	$p_f$ correction parameter MeV/ $c$
1.1	3146.41(3)	32.46(8)	2.22(8)
1.4	3147.35(3)	35.56(7)	1.94(6)
1.6	3148.45(3)	39.00(6)	1.69(6)
2.1	3150.42(3)	44.09(6)	1.57(5)
2.6	3152.45(3)	49.25(5)	1.35(5)
3.1	3154.49(3)	53.66(5)	1.28(4)
4.1	3158.71(3)	61.70(5)	1.07(5)
5.1	3162.78(3)	68.77(4)	0.95(4)
6.3	3168.05(3)	76.92(4)	0.88(3)
7.3	3172.15(3)	82.64(5)	0.84(4)
8.6	3177.51(3)	89.81(4)	0.76(4)
10.4	3184.87(3)	98.64(4)	0.74(4)

The extrapolation of the data to threshold is illustrated in Fig. 10 for both  $p_f$  and  $p_f^2$  versus  $p_d$ . Whereas, to first order,  $p_f^2$  depends linearly on  $p_d$ , the analysis considers the full dependence  $p_f = p_f(m_\eta, S, p_d)$ , as given by Eqs. (1) and (2). Only the  $\eta$  mass, chosen as a free parameter, defines the production threshold. The scaling factor  $S$ , discussed in Sec. II, allows for a possible systematic energy dependence of  $p_f$ . This would represent yet a further fine tuning of the description of the measurement process but it is crucial to note that its introduction does not affect the value obtained for the threshold momentum and hence  $m_\eta$ .

The overall fit to the data in Fig. 10 has a  $\chi^2/\text{NDF} = 1.28$  and the best value of the mass quoted in Table II is  $m_\eta = (547.873 \pm 0.005)$  MeV/ $c^2$ , where the error is primarily statistical. The corresponding deuteron momentum at threshold is  $p_d = (3141.688 \pm 0.021)$  MeV/ $c$ . A linear fit of  $p_f^2$  versus  $p_d$  would give a poorer reduced  $\chi^2$  and a mass that was 10 keV/ $c^2$  higher.

The scaling factor  $S = 1.008 \pm 0.001$  is well determined

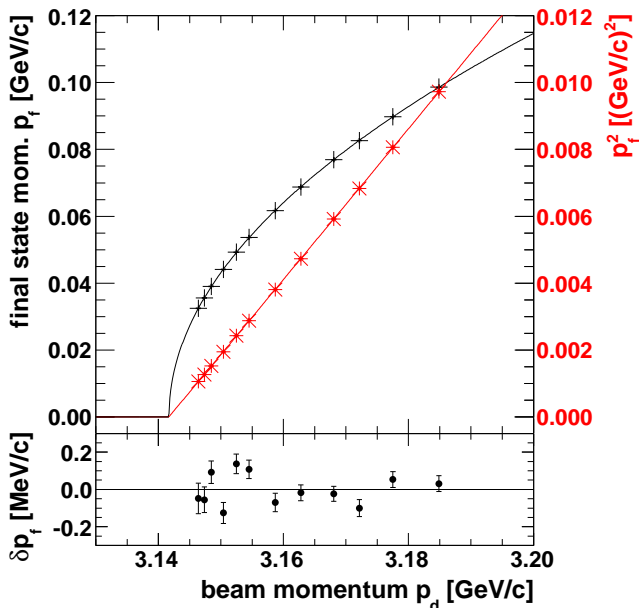


FIG. 10: (color online) Corrected values of the final-state c.m. momentum  $p_f$  (black crosses) and its square (red stars) plotted against the deuteron laboratory momentum  $p_d$ . The error bars are too small to be shown on the figure. The extrapolation to threshold is carried out on the basis of Eq. (1), where a scaling factor  $S$  has been introduced. The lower panel shows the deviations of the experimental data from the fitted curve in  $p_f$ . The errors shown here do not include the overall systematic uncertainty in  $p_f$  associated with the description of the profile in Fig. 8.

TABLE II: Values of the  $\eta$ -mass and scaling factor evaluated separately for the two supercycles and for the complete data set. The errors do not include the systematic uncertainties in the determination of the beam momentum.

Supercycle	Scaling factor $S$	$m_\eta$
1	$1.008 \pm 0.001$	$(547.870 \pm 0.007) \text{ MeV}/c^2$
2	$1.008 \pm 0.001$	$(547.877 \pm 0.007) \text{ MeV}/c^2$
1+2	$1.008 \pm 0.001$	$(547.873 \pm 0.005) \text{ MeV}/c^2$

and differs very slightly from unity, which means that the twelve momentum spheres are about 0.8% bigger than expected. One consequence of this is that the missing mass is not constant and one would get a slightly different value at each of the twelve energies studied. If one took  $S = 1.0$ , the  $\chi^2/\text{NDF}$  would jump to 24.7 and this would result in a shift of  $64 \text{ keV}/c^2$  in the  $\eta$  mass. Such a systematic error is avoided in the threshold-determination method described in Sec. II.

By far the dominant systematic errors arise from the determinations of the absolute value of the beam momentum and the  $p_f$  correction parameters. As can be seen from Table III, all other sources, such as effects from the time stability of the data, further contributions from the fine calibration, the event selection, the background sub-

traction for the  $p_f$  distributions, as well as contributions of the  $\eta$  mass assumed in Monte Carlo simulations, are negligible in comparison.

TABLE III: Systematic uncertainties in the determination of  $m_\eta$ . The small “experimental settings” contribution includes effects from the magnetic field, the deflection angle, and the (vertical) wire chamber positions, all of which are coupled. The PDG value of  $m_\eta$  [5] was used in the simulations but, if our result were used, it would only result in a  $2 \text{ keV}/c^2$  change. The effects of putting stricter cuts on  $\Delta E \times \beta^2$  and the flight length are also shown.

Source	Variation	$\Delta m_\eta$ $\text{keV}/c^2$
Absolute beam momentum	$95 \text{ keV}/c$	23
Experimental settings		2
$m_\eta$ assumed in simulations	$20 \text{ keV}/c^2$	< 2
$\Delta E \times \beta^2$ cut	$6\sigma \rightarrow 2\sigma$	5
Flight length cut	$3\sigma \rightarrow 2\sigma$	1
$p_f$ correction parameters	$4\sigma \rightarrow 2\sigma$	12
Total systematic uncertainty		27

This uncertainty in the beam momentum translates into one in the mass of

$$\Delta m_\eta = \frac{m_p p_d}{(m_{^3\text{He}} + m_\eta) E_d} \Delta p_d = 23 \text{ keV}/c^2, \quad (3)$$

and hence, taken together with all other systematic uncertainties, to a final value of

$$m_\eta = (547.873 \pm 0.005_{\text{stat}} \pm 0.027_{\text{syst}}) \text{ MeV}/c^2. \quad (4)$$

To investigate further some of the systematic effects, the results were extrapolated separately for the data obtained in the two supercycles and the individual values of the  $\eta$  mass and the scaling factor  $S$  are given in Table II. There is only a tiny difference between the two separately determined  $\eta$  mass values of  $7 \text{ keV}/c^2$ . This agreement supports the validity of taking the mean values of the beam momenta determined at the beginning and end of the measurements and the subsequent correct handling of the corresponding systematic uncertainties.

## VII. CONCLUSIONS

We have measured the mass of the  $\eta$  meson in a missing-mass experiment by identifying precisely the production threshold in the  $dp \rightarrow ^3\text{He} \eta$  reaction. As is seen in Fig. 11, the value obtained is consistent with all the recent measurements where the meson decay products were studied [1–4]. The precision achieved is similar to these works and the deviation from the PDG best value [5] is only  $20 \text{ keV}/c^2$ , which is less than our systematic error.

This success was based upon a precise determination of the beam momentum using the spin-resonance technique [11], a clear identification of the  $\eta$  signal [9], and a

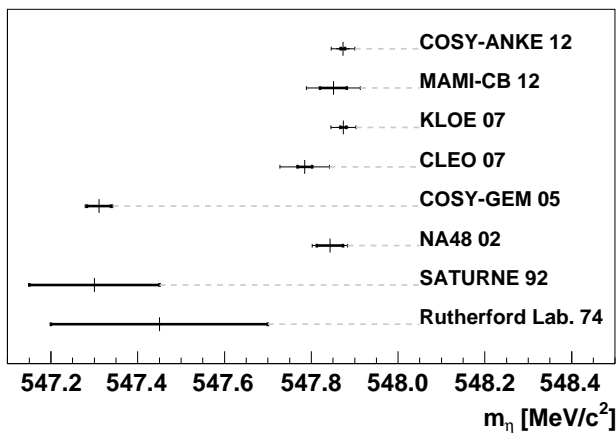


FIG. 11: Results of the different  $\eta$  mass experiments. Where two error bars are shown, the heavy line indicates the statistical uncertainty and the faint ones the systematic. The earlier missing-mass experiments, marked Rutherford Lab. 74 [6], SATURNE 92 [7], and COSY-GEM 05 [8], all obtained low values of  $m_\eta$  compared to the experiments where the meson was identified through its decay products, viz. NA48 02 [1], KLOE 07 [2], CLEO 07 [4], and MAMI-CB 12 [3]. Our result, COSY-ANKE 12, is completely consistent with these more refined experiments.

systematic study of the measurement of the  ${}^3\text{He}\eta$  final-state momentum in the ANKE spectrometer. The latter was made possible only through the complete geometric acceptance of ANKE for the  $dp \rightarrow {}^3\text{He}\eta$  reaction close to threshold. This allowed us to require that the c.m. momentum in the final state should be identical in all directions. This is a powerful technique that might be useful for other two-body reactions. Unlike the MAMI methodology [3], the experiment relied purely upon kinematics

rather than yields to determine the threshold momentum and hence the meson mass. However, it is important to realize that the anomalous behavior of the production cross section, where the cross section jumps so rapidly with excess energy, leads to the desirable high count rates near threshold.

Our result differs by about  $0.5 \text{ MeV}/c^2$  from earlier missing-mass evaluations [6–8] and so the hypothesis of a distortion of the background under the  $\eta$  peak must be discarded. Unlike experiments with external targets, the energy loss in a windowless cluster jet is negligible, but the current experiment had other advantages over these measurements. In particular, if we had access only to data taken in the forward direction, this would not have allowed the fine tuning of the spectrometer and a somewhat different value would have been found for  $m_\eta$ .

Finally, twelve energies above threshold were investigated and this allowed a reliable extrapolation to be made to find the production threshold. This is intrinsically subject to far fewer systematic uncertainties than a measurement at a single energy. It is therefore clear that, with care, a missing-mass approach can be competitive with experiments in which meson decays are measured.

#### Acknowledgments

The authors wish to express their thanks to the other members of the COSY machine crew for producing such good experimental conditions and also to the other members of the ANKE collaboration for diverse help in the experiment. This work was supported in part by the JCHP (Fremde Forschungen und Entwicklungsarbeiten) FFE.

- 
- [1] A. Lai *et al.*, Phys. Lett. B **533**, 196 (2002).  
 [2] F. Ambrosino *et al.*, J. High Energy Phys. **12**, 73 (2007).  
 [3] A. Nikolaev, Ph.D. thesis, University of Bonn (2012), available from <http://hss.ulb.uni-bonn.de/2012/2764/2764.htm>; MAMI-CB experiment, submitted for publication.  
 [4] D. H. Miller *et al.*, Phys. Rev. Lett. **99**, 122002 (2007).  
 [5] K. Nakamura *et al.* (Particle Data Group), J. Phys. G **37**, 075021 (2010).  
 [6] A. Duane *et al.*, Phys. Rev. Lett. **32**, 425 (1974).  
 [7] F. Plouin *et al.*, Phys. Lett. B **276**, 526 (1992).  
 [8] M. Abdel-Bary *et al.*, Phys. Lett. B **619**, 281 (2005).  
 [9] T. Mersmann *et al.*, Phys. Rev. Lett. **98**, 242301 (2007).  
 [10] T. Rausmann *et al.*, Phys. Rev. C **80**, 017001 (2009).  
 [11] P. Goslawski *et al.*, Phys. Rev. ST Accel. Beams **13**, 022803 (2010).  
 [12] NIST - National Institute for Standards and Technology, <http://physics.nist.gov/cuu/Constants/index.html>.  
 [13] Ya. S. Derbenev *et al.*, Part. Accel. **10**, 177 (1980).  
 [14] R. Maier *et al.*, Nucl. Instrum. Methods Phys. Res. Sect. A **390**, 1 (1997).  
 [15] S. Barsov *et al.*, Nucl. Instrum. Methods Phys. Res. Sect. A **462**, 364 (2001).  
 [16] A. Khoukaz *et al.*, Eur. Phys. J. D **5**, 275 (1999).  
 [17] B. Chiladze *et al.*, Phys. Part. Nucl. **113**, 95 (2002).  
 [18] S. Dymov *et al.*, Phys. Part. Nucl. **119**, 40 (2004).  
 [19] S. Dymov, ANKE Notes No. 22: FD Momentum Calibration for March'08 Beam Time (2009), available from [www2.fz-juelich.de/ikp/anke/en/internal.shtml](http://www2.fz-juelich.de/ikp/anke/en/internal.shtml).  
 [20] A. Khoukaz, COSY Proposal + Beam Request No. 187, available from [www2.fz-juelich.de/ikp/anke/en/proposals.shtml](http://www2.fz-juelich.de/ikp/anke/en/proposals.shtml).